Nanocomposite Hydrogels Enhanced by Cellulose Nanocrystals Stabilized Pickering Emulsions with Self-Healing Performance in Subzero Environment

Qichao Fan
Ludong University
Bencai Lin
Changzhou University
Yu Nie
Ludong University
Qing Sun
Ludong University
Wenxiang Wang
Ludong University
Liangjiu Bai (bailiangjiu@ldu.edu.cn)
Ludong University https://orcid.org/0000-0002-4997-627X
Hou Chen
Ludong University
Lixia Yang
Ludong University
Huawei Yang
Ludong University
Donglei Wei
Ludong University

Research Article

Keywords: Cellulose nanocrystals, Pickering emulsions, Anti-freezing, Self-healing hydrogels

Posted Date: April 27th, 2021

DOI: https://doi.org/10.21203/rs.3.rs-410447/v1

Version of Record: A version of this preprint was published at Cellulose on August 3rd, 2021. See the published version at https://doi.org/10.1007/s10570-021-04120-1.

Abstract

Nowadays, hydrogels as flexible materials have attracted considerable attention in frontier fields such as wearable electronic devices, soft actuators and robotics. However, most hydrogels use water as matrix will inevitably freeze at subzero and damage in severe environment, which greatly reducing their service life and practical value. Herein, nanocomposite hydrogels with self-healing performance at subzero temperatures were proposed by introducing binary water-glycerol continuous phase and dual self-healing interactions. The efficacy of binary solvents was emphasized in preventing formation of ice crystals, enhancing flexible and self-healing abilities of hydrogels in subzero environment. Particularly, linseed oil (LO) as healing agent was effectively loaded in Pickering droplets by cellulose nanocrystals (CNCs). Due to external healing agent and non-covalent bonding, hydrogels showed good self-healing performance at subzero temperature (the healing efficiency could be up to 80.1% for 12 h at -20 ℃). Thus, the designed hydrogels demonstrated multifunctional properties to overcome adverse conditions, which greatly elevated their durability and practicality.

Introduction

As an ideal candidate for soft materials, hydrogels have caught great interest due to unique electrical, flexible and tensile properties (Chen et al. 2020c; Shi et al. 2020). Varied hydrogels have developed rapidly and been universally applied in many advanced areas, such as artificial skin (Lei and Wu 2018), wearable electronic equipment (Buenger et al. 2012), drug carrier (Song et al. 2021) and tissue engineering (Zhao et al. 2020). The most representative characteristic of hydrogels is the ability to absorb and retain large amounts of water without dissolving under three-dimensional structure (Li et al. 2016). However, conventional hydrogels rely on water as matrix, inevitably freeze at subzero temperatures, resulting in irreversibly damaged structure of polymer network (Wang et al. 2019b; Wei et al. 2020). Specially, owing to rigid aqueous phase, hydrogels lose the flexible ability and could be easily destroyed, which threatens their service life and practical value. Thus, it is necessary to endow hydrogels with the performance of self-healing in subzero environment to resist external interference, which will broaden their underlying applications in a wider temperature range.

The cold resistance mechanisms in natural organisms provide wealth strategies for improving the frost resistance. Inspired by the phenomenon of increasing intracellular solute concentration to impede ice formation in natural plants, binary solvent system attracted a strong interest (Xu et al. 2020). Generally, these solvent systems involve two components with entirely opposite physiochemical properties, like water and organism (Zhang et al. 2018). Glycerol, with the merits of non-toxic and solving with water in any ratio, is commonly served as cryoprotective agent (Chen et al. 2020a; Yu et al. 2021). The strong hydrogen bonds formed between glycerol and water compete with the hydrogen bonds formed in water, thus reducing the hydrogen bond density between water molecules, which destroy ice crystal lattices and reduce freezing point (Liao et al. 2019). For instance, Yang et al. (Yang et al. 2019) designed anti-freezing hydrogels by introducing polyelectrolytes and glycerol, which could maintain excellent conductivity and self-healing properties at -20°C for 24 h. Ge et al. (Ge et al. 2020) proposed muscle-inspired hydrogel

bioelectronic devices that possessed high stretchability, desirable sensitivity, durable adhesion feature and self-healing performance at low temperature, ascribing to glycerol/water binary solvent system. Thus, the anti-freezing property could be easily obtained by constructing facile and efficient water-glycerol system, contributing to preserving original performance in subzero environment.

Furthermore, polymer chains within hydrogels lack fluidity at low temperatures, which leading weak network to resist damages by deformation, further cripple mechanical properties and realistic applications (Lu and Chen 2020). Inspired by autonomously healing phenomenon of natural skin, self-healing mechanisms in hydrogels have attracted numerous attentions (Lin et al. 2019; Son et al. 2018). Self-healing hydrogels exhibit excellent durability and mechanical properties that can autonomously heal damages or nonautonomously with external stimuli (Li et al. 2017b; Taylor and In Het Panhuis 2016). Self-healing mechanisms could be classified into extrinsic and intrinsic types according to the healing process. Extrinsic healing is realized with the participation of external healing agents, whereas intrinsic healing is based on dynamic reversible physicochemical action, like non-covalent and covalent interactions (Liu et al. 2019). Combining these two approaches can build double-healing construction, as well as obviously increase healing efficiency at low temperatures. Notable, Pickering emulsions (Wu and Ma 2016) stabilized by cellulose nanocrystals (CNCs) (Wang et al. 2020) has caught much attention, providing an effective strategy to store and release healing agent (Li et al. 2018). CNCs are considered suitable candidates as biomass solid emulsifiers, reflecting the advantages of high aspect ratio, small size, intermediate wettability, non-toxicity, biocompatibility and sustainable (Zhang et al. 2019). Fortunately, linseed oil (LO) with attractive virtues such as non-toxic, easily manage and the ability to fill cracks by polymerization with oxygen, showing promising applications as external healing agent encapsulated in Pickering droplets (Jadhav et al. 2011; Navarchian et al. 2019). Recently, studies on preparing self-healing materials based on LO as healing reagent in Pickering droplets have been reported. Li et al. (Li et al. 2019) designed Poly(urea – formaldehyde)/SiO_2 hybrid microcapsules to load LO by in situ polymerization and Pickering emulsion template, which endowing coatings with excellent self-healing and self-lubricating properties. Li et al. (Li et al. 2017a) fabricated graphene oxide microcapsules (GOMCs) with nanometer-thick shells by Pickering emulsions and applied in waterborne polymer composite coatings, where LO loaded in GOMCs imparted self-healing properties and retarded the corrosion process.

Herein, the composite hydrogels with enhanced self-healing performance at low temperatures were designed through binary solvent system and dual self-healing interactions. Facile one-pot thermal method was utilized for the construction of polyacrylic acid (PAA) skeleton. LO as external healing agent was encapsulated in Pickering droplets with CNCs as solid emulsifiers. In view of CNCs and LO were all biomass materials, this strategy provided a simple and green way to load the healing agent. The introduction of glycerol ensured the characters of anti-freezing, water retention and flexibility of hydrogels. Double self-healing interactions were composed of two aspects. On the one hand, LO could be released from Pickering droplets and polymerization with oxygen. The other was realized with reversible

dynamic non-covalent bonding, including hydrogen bonds and the chelation of Fe^{3+}. Overall, the obtained hydrogels were comprehensively characterized and showed great potentials as flexible materials.

Experimental

Materials

Acrylic acid (AA, ≥ 98.0%, M_n = 72.06 g mol^{-1}), iron (Ⅲ) chloride hexahydrate ($FeCl_3 \cdot 6\ H_2O$, ≥ 99.0%, Mw = 270.29 g mol^{-1}) and ethanedioic acid dihydrate (≥ 99.5%, Mw = 126.07 g mol^{-1}) were obtained from Sinopharm. Choline chloride (≥ 98.0%, Mw = 139.62 g mol^{-1}) was obtained from Macklin. Potassium peroxydisulfate (KPS, ≥ 99.5%, Mw = 270.32 g mol^{-1}) was obtained from Damao Reagent. Glycerol (≥ 99.0%, Mw = 92.09 g mol^{-1}) was obtained from Fuyu Chemical. LO (≥ 99.0%, 0.93 g mL^{-1}) was obtained from Greeno. $FeCl_3 \cdot 6\ H_2O$ was dissolved in distilled water to obtain Iron (Ⅲ) solution (12.0 mg mL^{-1}). Potassium peroxydisulfate was dissolved in distilled water to obtain KPS solution (6.6 mg mL^{-1}). The other reagents were directly used without further transforming.

Extraction of CNCs

CNCs were extracted by acid hydrolysis procedure according to our previous research (Fan et al. 2020). 0.25 g of cellulose, 15.3 g of ethanedioic acid dihydrate and 9.7 g of choline chloride were added in a flask, stirring at 350 r/min at 100 ℃ for 5 h. The mixture was centrifuged by adding distilled water for about 3 times, then dialyzed and freeze-dried.

Preparation of Pickering emulsions

0.02 g of CNCs and 6.0 mL of distilled water was added in a vial and ultrasonic for 10 minutes to obtain milky white CNCs suspension. Then, 150.0 μL of LO was added and stirring at 8000 r/min for 3 minutes to obtain Pickering emulsions.

Synthesis of hydrogels

4.0 mL of AA, 5.0 mL of KPS solution, 1.0 mL of Iron (Ⅲ) solution, different doses of Pickering emulsions and glycerol were added in a vial, then ultrasonic for 10 minutes to obtain uniformly dispersed mixture. The mixture was polymerized at 65 ℃ with stirring at 350 r/min for 15 minutes. Hydrogels were formed in a mold at 40 ℃ for a period of time. The hydrogels were marked as HG-P_xG_y, where x represented the content of Pickering emulsions and y represented the content of glycerol.

Evaluation of water retention and swelling abilities

The hydrogels were molded in circle shape (Φ = 2.5 cm), then cut in average sections for measurements. To explore water retention capacity, the samples were kept at 25, 45 and 65 ℃ for 7 days. The reduction of water content in hydrogels was reflected according to the following formula: W_t/W_0 (%), where W_t was

the weight at t time and W_0 was the original weight. In addition, the same size hydrogels were immersed in distilled water (pH = 6.5) at 25 ℃, then the samples were taken out and dried by filter paper to weight every 20 minutes. The increment of water content in hydrogels was calculated by the following equation: W/W_0 (%), where W was the change of weight and W_0 was the original weight.

Evaluation of self-healing performance at subzero temperature

The subzero temperature of -20 ℃ was provided by a low constant temperature bath (DC-2006, SHP, -20 ~ 95 ℃). The self-healing ability was performed on Stress(σ)-Strain(ε) curves supported by tensile machine (LDW, Songdun). The regular dumbbell-shaped samples were cut in half and healed at -20 ℃ without external stimuli, then immediately used for testing at room temperature. With different healed time and different doses of Pickering emulsions, the healed samples were stretched at a uniform speed of 50 mm/min. Additionally, the self-healing efficiency was calculated by σ/σ_0, where σ was the fracture stress of healed hydrogels and σ_0 was the fracture stress of initial hydrogels.

Characterization and methods

The morphology of CNCs was obtained from transmission electron microscope (TEM, Thermo Fisher Scientific Talos F200X G2) and scanning electron microscope (SEM, Hitichi SU-8010). The cross-sectional of hydrogels were performed on SEM. Surface charge of CNCs was tested via zeta potential measurement (Zetasizer Nano ZS90, Britain Malvern). The structural information was conducted on Fourier transform infrared (FT-IR, Nicolet500) and x-ray photoelectron spectroscopy (XPS, Escalab Xi+). The UV–vis spectra were recorded in the 190–500 nm wavelength range using SolidSpec-3700 at room temperature. The healing process of hydrogels and morphology of emulsions were recorded by optical microscope (DMM-300C). Rheological curves were recorded by rheometer (TA DFR-2). The freezing points of hydrogels were investigated by differential scanning calorimeter (DSC, Netzsch 204 F1).

Results And Discussion

General preparation process of Pickering emulsions was to disperse solid particles in water phase, and then added oil phase to form emulsions under high-speed mixing. The schematic of CNCs-stabilized Pickering emulsions was illustrated in Scheme 1a. At present, recognized stabilization mechanism of Pickering emulsions mainly concentrated on solid particles adsorbing at the oil-water interface and forming monolayer or multilayer film. The existence of interfacial layers could effectively prevent droplets aggregation and condensation (Low et al. 2020).

The emulsifying efficiency was affected by many factors, which mainly depended on the properties of solid emulsifier. With numerous active groups and high aspect ratio, CNCs can form the particle layer and reflect affinity for both phases, which enable droplets preserved during polymerization process (Jiang et al. 2020). The quality of CNCs were firstly characterized and discussed. Deep eutectic solvents (DESs), composited of hydrogen bond donors and hydrogen bond acceptors in a certain ratio, has been used as hydrolytic medium to degrade the amorphous regions in cellulose (Douard et al. 2021; Sirviö et al. 2015).

Due to green, less toxic and easily obtained, DESs method was used in the extraction and modification of CNCs. In this way, CNCs were modified with hydrophilic carboxyl groups, resulting in satisfactory dispersion. Meanwhile, the existence of active carboxyl groups could improve the hydrophilicity of CNCs, contributing to reduce surface energy of the phases (Chen et al. 2020b; Hong et al. 2020a).

From TEM and SEM images (Fig. 1a, Fig. S1), CNCs were rod-like particles with the length of 187.0 ± 37.4 nm and diameter of 17.6 ± 4.0 nm. From FT-IR spectra (Fig. S2), typical characteristic peaks of cellulose at 3340 cm^{-1}, 2900 cm^{-1}, 1320 cm^{-1} and 1050 cm^{-1} were O-H stretching, C-H stretching, O-H bending and C-O-C pyranose ring stretching vibration, respectively (Hong et al. 2020b; Jordan et al. 2019). The spectra of cellulose and CNCs showed similar peaks, but a new slight peak located at 1730 cm^{-1} was observed, which attributing to carboxyl group (Ling et al. 2018). This peak indicated that weak esterification occurred between carboxyl groups in cellulose chains and oxalic acid (Li et al. 2020). Also, this was confirmed by XPS method. The wide scan spectra of cellulose and CNCs were shown in Fig. S3a. The carbon signal appeared at 286.5 eV, and the oxygen signal appeared at 532.8 eV. In Fig. S3b, the peaks at 286.5, 284.8, 289.5 and 288.1 eV corresponding to C–OH of alcohols, C–C/ C–H linkages, O–C = O of ester carbon and O-C-O, respectively (Oliveira et al. 2016). Additionally, from Fig. S4, CNCs exhibited a relatively negative zeta potential at -27.3 mV, because of the presence of the carboxyl groups on the surfaces. These results demonstrated CNCs with attractive morphology and negative charged surface were suitable to be used as stabilizer for Pickering emulsions.

Then, CNCs suspension was used to prepare Pickering emulsions (Fig. 1b). After adding LO and under high-speed homogenization, the creamy O/W emulsions were synthesized (Fig. S5). Even after leaving at room temperature for 1 day, no obvious grease was found in the stable system. On the other hand, to further study the effect of CNCs content and oil-water ratio on emulsions stability, different types of Pickering emulsions were observed via optical microscope images (Fig. S6). In a certain content of CNCs (0.33 wt%), the size of Pickering droplets has increased with oil-water ratio raised. The same phenomenon occurred when the content of CNCs reduced from 0.50 to 0.17 wt% at the oil-water ratio of 1:40. The results showed that the size of droplets was related to increasing oil-water ratio or reducing CNCs contents, ascribing to small amounts of particles covering the surface of LO to form dense interface layers, which leaving the droplets in an unstable state (Wang et al. 2019a).

Rheology tests were further applied to investigate the stability of emulsions (Farias et al. 2020; Maestro et al. 2020). With frequency sweep data increased from 0.1 to 200 rad/s, both of the values of modulus improved, which manifested non-Newtonian fluidlike behavior (Fig. 1c) (Alam et al. 2008). With strain sweep data from 1 to 1000%, two curves showed a downward trend and G' was in a greater range (Fig. 1d). Before the intersection, G' was greater than G", suggesting the emulsions were in a stable gel-type structure. When strain continued to increase, gel structure was destroyed and the emulsions were in an unstable liquid state. The point where two curves intersected was at 60%, which represented the maximum strain value that the emulsions could bear (Debeli et al. 2020). Besides, the values of G' and G" showed monotonicity over time (Fig. 1e). G' (0.12 Pa) still dominated over G" (0.03 Pa) from 0 to 200 s, manifesting the emulsions could remain stable for a long time (Liu et al. 2017).

Next, hydrogels were synthesized through facile and simple one-pot method (Scheme. 1b). A certain percentage of Pickering emulsions, Iron (Ⅲ) solution, KPS solution, glycerol and AA were added in the vial and sonicated to obtain well-dispersed mixture. Then, the polymerization process was completed during 65 ℃ with stirring for 15 minutes. Poly (acrylic acid) (PAA) networks were constructed by conventional free radical polymerization of acrylic acid in aqueous system (Fernandes et al. 2015), which was composed of water as matrix, AA as monomer and KPS as initiator. The polymerization produced strong chemical cross-linked backbone, while Fe^{3+} further developed the network through physical crosslinking (Wei et al. 2013). As shown in Fig. S7, the transformation process from solution to gel was well visualized. At the beginning of the reaction, the system was in a fluid state. After the reaction, the hydrogels with stable and uniform state were obtained.

In order to analyze the internal structure and surface morphology, hydrogels were freeze-dried and observed by SEM. As shown in Fig. 2a and Fig. S8, compared with HG-P_0G_0, HG-$P_{1.0}G_0$ demonstrated porous three-dimensional networks with uniform apertures of 21.3 ± 5.4 μm. This was owing to noncovalent bonding interaction between Pickering droplets and PAA chains, which increased entanglement density within hydrogels. Obviously, HG-$P_{1.0}G_{1.0}$ exhibited a more firm and smooth structure with the smaller apertures of 8.9 ± 2.1 μm (Fig. 2b). The introduction of glycerol provided abundant hydroxyl groups, contributed to improve the hydrogen bonds and interaction between polymer chains. The uniform pores with smaller sizes signified that hydrogels possessed dense networks, which leading to higher mechanical properties (Lin et al. 2021).

The porous three-dimensional network endowed hydrogels with the abilities to absorb and retain a certain amount of water. Figure 2c showed the swelling kinetics curves of hydrogels with different content of Pickering emulsions immersed in distilled water at room temperature. The swelling rate increased rapidly in the first 120 minutes, on account of substantial water molecules were quickly fill internal porous channels. After that, the swelling rate slowed down until it reached dynamic equilibrium. At the same immersion time, water absorption was related to emulsions content. As Pickering emulsions increased from 0.5 to 1.0 and 1.5 mL, the water absorption changed from 269.4–234.1% and 192.1%, respectively. These results demonstrated that the denser and stable structures within hydrogels were enhanced by Pickering droplets, which was consistent with the SEM and mechanical results. The tenacious internal network prevented the structures from collapsing due to excessive water absorption. Besides, water retention kinetics curves of hydrogels at 25, 45 and 65 ℃ were shown in Fig. 2d. At 45°C and 65°C, the water content dropped rapidly within the first two days. The water retention was related to temperatures that high temperature accelerated water evaporation. After 7 days, the weight retention ratio at 25, 45 and 65 ℃ was 86.2%, 70.7% and 65.1%, respectively. By comparison, HG-$P_{1.0}G_0$ could only maintain 57.2% of their original weight. The water content determined fluidity of polymer chains further flexibility of hydrogels, and glycerol was underscored as a crucial factor that retarded evaporation process.

To verify the low-temperature tolerance performance, the freezing points of hydrogels were obtained from DSC thermograms in Fig. 2e. Interestingly, HG-$P_{1.0}G_0$ showed a sharp exothermic peak at -17 ℃, which

was far below the freezing point of pure water. Because PAA chains provided a wide platform to form hydrogen bonds with water molecules, inhibiting the formation of ice crystals (Deller et al. 2014). After introducing glycerol, freezing point of HG-$P_{1.0}G_{1.0}$ was depressed at -40 ℃ as well as the exothermic peak became smaller and broader, which intuitively proved that binary water-glycerol system bestowed hydrogels with freezing tolerance attribute (Lin et al. 2021). Additionally, the anti-freezing performance were characterized by optical photographs in Fig. 2f. All hydrogels presented flexibility that could be easily bent at 25 ℃. After being placed at -20 ℃ for 24 hours, HG-$P_{1.0}G_0$ were in a frozen solid-like state that could not be bent. Inversely, HG-$P_{1.0}G_{1.0}$ showed good anti-freezing ability that no ice area was observed and still could be bent.

The hydrogels possessed excellent self-healing performance depended on double healing interactions (Scheme 1c). PAA chains with rich active carboxyl groups on building the three-dimensional network structure and providing connection sites. When hydrogels were cracked, the healing process was carried out by reversible noncovalent interactions, including vigorous hydrogen bonding and metal ions-coordination. Hydrogen-bond interactions were widely existed between oxygen-containing groups of Pickering droplets, PAA, water and glycerol. Self-healing mechanisms based on hydrogen bonds have been widely reported (Chen et al. 2018; Dai et al. 2015; Phadke et al. 2012). For example, Li et. al prepared double-network hydrogels composed of PEG and PVA, while the self-healing ability resulted from hydrogen bonding between the hydroxyl side groups (Li et al. 2015). And the coordinate interactions of Fe^{3+} was confirmed by UV-vis. As shown in Fig. S9a, AA solution showed a characteristic peak at 195 nm. After introducing Fe^{3+}, the characteristic peak was shifted to 203 nm, which indicated the chelation interactions existed between Fe^{3+} and hydroxyl groups (Rao et al. 2016).

Benefiting from LO broken from Pickering droplets, the self-healing efficiency was further enhanced. LO as healing agent was encapsulated in microcapsules has been widely used in self-healing coating (Lang and Zhou 2017). This was because it contained unsaturated fatty acids, which provided lots of C = C bonds. In the presence of oxygen, LO could rapidly oxidized to form a solid film and fill the cracks (Suryanarayana et al. 2008). The ability of LO as external healing regent was confirmed by FT-IR spectra (Fig. S9b). The fresh LO had an absorption peak at the wavelength of 1652 cm^{-1}, attributing to the transitions of C = C bonds. For the LO/PAA hydrogels, this characteristic peak disappeared, suggesting that LO polymerized with oxygen in hydrogel matrix (Fan et al. 2019). The release of LO from Pickering droplets were recorded by UV-vis spectra. Firstly, absorbance versus concentration calibration curve of LO dissolved in petroleum ether was obtained (Fig. S9c). In Fig. S9d, LO showed characteristic peaks in ultraviolet region. The concentrations of LO were calculated as 2.64×10^{-6}, 1.65×10^{-5} and 1.98×10^{-5} mol/L at the time of 4, 8 and 12 h, respectively, which exhibited a slowly release process within hydrogels. These results indicated that LO could be used as healing regent as well as effectively encapsulated in Pickering droplets.

The self-healing properties of hydrogels in subzero environment were demonstrated via typical stress-strain curves. It was well known that the shape and size of the samples influenced the tensile data,

hydrogels were made strictly into the standard templates (Fig. 3a). The effects of Pickering emulsions and healing time on mechanical abilities and self-healing efficiency were proved in Fig. 3b-d. With increasing Pickering emulsions contents of 0, 0.5, 1.0 and 1.5 mL, the corresponding healing efficiency was 57.1, 71.0, 80.1 and 76.9% for 12 h. Similarly, the value of stress also showed a trend of increasing then decreasing. With addition of certain contents of Pickering droplets, polymer chains within hydrogels entangled tightly and caused denser structure, leading to higher mechanical properties and healing efficiency. However, excess Pickering droplets prevented the construction of hydrogen bonds between polymer chains, and the presence of polymer films at cracks may reduce the effect of reversible non-covalent bonding, resulting in a loose network structure. Besides, as the healing time were 4, 8 and 12 h, the corresponding healing efficiency were 21.3, 44.9 and 80.1%. The efficiency was noticeably improved with healing time increased, which implying more non-covalent bonds were rearranged. The strain of original HG-$P_{1.0}G_{1.0}$ was 1900% and stress was 0.24 MPa at -20 ℃, which also reflected reliable stretchable and anti-freezing characters. For comparison, the healing performance was assessed at room temperature that hydrogels were cut and self-healing for 12 h. The self-healing efficiency of HG-$P_0G_{1.0}$ and HG-$P_{1.0}G_{1.0}$ were 64.7% and 90.0%, respectively (Fig. S10). These results were higher than those at -20 ℃, because the fluidity of polymer chains and active groups at high temperatures facilitated the healing process.

Furthermore, the self-healing ability and energy dissipation process were evaluated by loading-unloading stress-strain curves under 100% strain for ten successive cycles without waiting (Fig. 3e-f). The hysteresis loops revealed larger areas during the 1st to 3rd process, which indicated that energy consumption was mainly in the previous cycles. Because of the broken bonds within healed hydrogels were partially restored, the stress value was lower than original hydrogels (Ma et al. 2020). Even after ten successive cycles, the value of stress remained at 69.5% as compared with the first cycle. These results showed that the hydrogels possessed anti-fatigue properties, which rose from the double self-healing interactions.

Macroscopically, the self-healing ability and mechanical properties of hydrogels were characterized by optical photographs. The hydrogels were dyed by Prussian blue and Rhodamine B, respectively. In Fig. 3g, two different colors of hydrogels were molded in circle shapes (Φ = 2.5 cm), then, cut in half and healed at -20 ℃ for stretching. The samples could be stretched to a certain length. In a same way, the dyed hydrogels were cut into standard dumbbell shapes and broken down in the middle. Different color sections were stuck together and healed at -20 ℃. The healed samples could be stretched out by 20 cm and withstand up to a weight of 200 g (Fig. 3h-i), due to the tight healing layer formed at cracks. To further confirm this, linear cracks were scratched on the surface of hydrogels and then exposed to -20 ℃ environment, while the morphology of healing areas were recorded by microscopic images. It was found that all of the separate sections gradually merged closely, as well as the color of scratches became lighter and size became smaller. The traces were clearly observed on HG-$P_0G_{1.0}$ at healing time of 0, 1 h, 4 h and 8 h (Fig. S11a-d). With the participation of Pickering droplets, HG-$P_{1.0}G_{1.0}$ showed a markedly enhanced healing process that the cracks disappeared on the surface after 8 hours (Fig. S11e-h). All the results

demonstrated brilliant self-healing and flexibility performance of nanocomposite hydrogels in subzero environment.

Conclusions

In summary, the durable nanocomposite hydrogels were successfully synthesized by an ingenious strategy, which templating on Pickering emulsions and binary water-glycerol system. The obtained hydrogels showed attractive stretchable, anti-drying, anti-freezing and self-healing characters. Highly self-healing efficiency profited from LO loaded in Pickering droplets and noncovalent bonding (metal ions-coordination and vigorous hydrogen bonds). Glycerol strongly locked water molecules and prevented the formation of ice crystals, played an active role in stretchable, moisturizing and anti-freezing. It was worth noting that the hydrogels could achieve 80.1% healing efficiency without external interventions at -20 ℃, meanwhile, the excellent mechanical properties (strain of 1900%, stress of 0.24 MPa) were preserved. Thus, we believe that these hydrogels possessed reliable durability and practicality to acclimatize for long service life, exhibiting great potentials in widespread applications as flexible materials.

Declarations

Acknowledgments

The research was financial supported by the National Natural Science Foundation of China (Nos. 51773086 and 51973086), the Key Program for Basic Research of Natural Science Foundation of Shandong Province (No. ZR2018ZC0946), the Project of Shandong Province Higher Educational Science (Nos. 2019KJA011 and J18KA080) and the Jiangsu Province Cultivation base for State Key Laboratory of Photovoltaic Science and Technology.

Compliance with Ethical Standards

This article does not contain any studies with human participants or animals performed by any of the authors.

Conflicts of Interest

There are no conflicts to declare.

References

1. Alam MM, Aramaki K (2008) Hexagonal phase based gel-emulsion (O/H_1 gel-emulsion): formation and rheology, Langmuir 24:12253-12259. https://doi.org/10.1021/la8021547
2. Buenger D, Topuz F, Groll J (2012) Hydrogels in sensing applications. Prog Polym Sci 37:1678-1719. https://doi.org/10.1016/j.progpolymsci.2012.09.001

3. Chen R, Xu X, Peng S; Chen J, Yu D, Xiao C, Li Y, Chen Y, Hu X, Liu M, Yang H, Wyman I, Wu X (2020a) A flexible and safe aqueous zinc–air battery with a wide operating temperature range from −20 to 70 °C. ACS Sustain Chem Eng 8:11501-11511. https://doi.org/10.1021/acssuschemeng.0c01111
4. Chen T, Chen Y, Rehman HU, Chen Z, Yang Z, Wang M, Li H, Liu H (2018) Ultratough, self-healing, and tissue-adhesive hydrogel for wound dressing. ACS Appl Mater Interfaces 10:33523-33531. https://doi.org/10.1021/acsami.8b10064
5. Chen Y, Zhu J, Yu H, Li Y (2020b) Fabricating robust soft-hard network of self-healable polyvinyl alcohol composite films with functionalized cellulose nanocrystals. Compos Sci Technol 194: 108165. https://doi.org/10.1016/j.compscitech.2020.108165
6. Chen Z, Yan T, Pan Z (2020c) Review of flexible strain sensors based on cellulose composites for multi-faceted applications. Cellulose 28:615-645. https://doi.org/10.1007/s10570-020-03543-6
7. Dai X, Zhang Y, Gao L, Bai T, Wang W, Cui Y, Liu W (2015) A mechanically strong, highly stable, thermoplastic, and self-healable supramolecular polymer hydrogel. Adv Mater 27:3566-3571. https://doi.org/10.1002/adma.201500534
8. Debeli DK, Lin C, Mekbib DB, Hu L, Deng J, Gan L, Shan G (2020) Controlling the stability and rheology of copolyol dispersions in fatty alcohol ethoxylate (AEO9)-stabilized multiple emulsions. Ind Eng Chem Res 59:18307-18317. https://doi.org/10.1021/acs.iecr.0c03792
9. Deller RC, Vatish M, Mitchell DA, Gibson MI (2014) Synthetic polymers enable non-vitreous cellular cryopreservation by reducing ice crystal growth during thawing. Nat Commun 5:3244. https://doi.org/10.1038/ncomms4244
10. Douard L, Bras J, Encinas T, Belgacem MN (2021) Natural acidic deep eutectic solvent to obtain cellulose nanocrystals using the design of experience approach. Carbohydr Polym 252:117136. https://doi.org/10.1016/j.carbpol.2020.117136
11. Fan D, Wang G, Ma A, Wang W, Chen H, Bai L, Yang H, Wei D, Yang L (2019) Surface engineering of porous carbon for self-healing nanocomposite hydrogels by mussel-inspired chemistry and PET-ATRP. ACS Appl Mater Interfaces 11:38126-38135. https://doi.org/10.1021/acsami.9b12264
12. Fan Q, Jiang C, Wang W, Bai L, Chen H, Yang H, Wei D, Yang L (2020) Eco-friendly extraction of cellulose nanocrystals from grape pomace and construction of self-healing nanocomposite hydrogels. Cellulose 27:2541-2553. https://doi.org/10.1007/s10570-020-02977-2
13. Farias BV, Brown D, Hearn A, Nunn N, Shenderova O, Khan SA (2020) Nanodiamond-stabilized Pickering emulsions: Microstructure and rheology. J Colloid Interface Sci 580:180-191. https://doi.org/10.1016/j.jcis.2020.07.030
14. Fernandes BS, Carlos Pinto J, Cabral-Albuquerque ECM, Fialho RL (2015) Free-radical polymerization of urea, acrylic acid, and glycerol in aqueous solutions. Polymer Engineering & Science 55:1219-1229. https://doi.org/10.1002/pen.24081
15. Ge G, Lu Y, Qu X, Zhao W, Ren Y, Wang W, Wang Q, Huang W, Dong X (2020) Muscle-inspired self-healing hydrogels for strain and temperature sensor. ACS Nano 14:218-228. https://doi.org/10.1021/acsnano.9b07874

16. Hong S, Song Y, Yuan Y, Lian H, Liimatainen H (2020a) Production and characterization of lignin containing nanocellulose from luffa through an acidic deep eutectic solvent treatment and systematic fractionation. Ind Crop Prod 143:111913. https://doi.org/10.1016/j.indcrop.2019.111913
17. Hong S, Yuan Y, Li P, Zhang K, Lian H, Liimatainen H (2020b) Enhancement of the nanofibrillation of birch cellulose pretreated with natural deep eutectic solvent Ind Crop Prod 154:112677. https://doi.org/10.1016/j.indcrop.2020.112677
18. Jadhav RS, Hundiwale DG, Mahulikar PP (2011) Synthesis and characterization of phenol-formaldehyde microcapsules containing linseed oil and its use in epoxy for self-healing and anticorrosive coating. J Appl Polym Sci 119:2911-2916. https://doi.org/10.1002/app.33010
19. Jiang H, Sheng, Y, Ngai T (2020) Pickering emulsions: versatility of colloidal particles and recent applications. Current Opinion in Colloid & Interface Science 49:1-15. https://doi.org/10.1016/j.cocis.2020.04.010
20. Jordan JH, Easson MW, Dien B, Thompson S, Condon BD (2019) Extraction and characterization of nanocellulose crystals from cotton gin motes and cotton gin waste. Cellulose 26:5959-5979. https://doi.org/10.1007/s10570-019-02533-7
21. Lang S, Zhou Q (2017) Synthesis and characterization of poly(urea-formaldehyde) microcapsules containing linseed oil for self-healing coating development. Prog Org Coat 105:99-110. https://doi.org/10.1016/j.porgcoat.2016.11.015
22. Lei Z, Wu P (2018) A supramolecular biomimetic skin combining a wide spectrum of mechanical properties and multiple sensory capabilities. Nat Commun 9:1134. https://doi.org/10.1038/s41467-018-03456-w
23. Li F, Abdalkarim SYH, Yu H-Y, Zhu J, Zhou Y, Guan Y (2020) Bifunctional reinforcement of green biopolymer packaging nanocomposites with natural cellulose nanocrystal–rosin hybrids. ACS Applied Bio Materials 3:1944-1954. https://doi.org/10.1021/acsabm.9b01100
24. Li G, Zhang H, Fortin D, Xia H, Zhao Y (2015) Poly(vinyl alcohol)-Poly(ethylene glycol) double-network hydrogel: a general approach to shape memory and self-healing functionalities. Langmuir 31:11709-11716. https://doi.org/10.1021/acs.langmuir.5b03474
25. Li J, Feng Q, Cui J, Yuan Q, Qiu H, Gao S, Yang J (2017a) Self-assembled graphene oxide microcapsules in Pickering emulsions for self-healing waterborne polyurethane coatings. Compos Sci Technol 151:282-290. https://doi.org/10.1016/j.compscitech.2017.07.031
26. Li J, Mo L, Lu CH, Fu T, Yang HH, Tan W (2016) Functional nucleic acid-based hydrogels for bioanalytical and biomedical applications. Chem Soc Rev 45:1410-1431. https://doi.org/10.1039/c5cs00586h
27. Li K, Li H, Cui Y, Li Z, Ji J, Feng Y, Chen S, Zhang M, Wang H (2019) Dual-functional coatings with self-lubricating and self-healing properties by combining Poly(urea–formaldehyde)/SiO_2 hybrid microcapsules containing linseed oil. Ind Eng Chem Res 58:22032-22039. https://doi.org/10.1021/acs.iecr.9b04736

28. Li Q, Liu C, Wen J, Wu Y, Shan Y, Liao J (2017b) The design, mechanism and biomedical application of self-healing hydrogels. Chinese Chem Lett 28:1857-1874. https://doi.org/10.1016/j.cclet.2017.05.007
29. Li X, Li J, Gong J, Kuang Y, Mo L, Song T (2018) Cellulose nanocrystals (CNCs) with different crystalline allomorph for oil in water Pickering emulsions. Carbohydr Polym 183:303-310. https://doi.org/10.1016/j.carbpol.2017.12.085
30. Liao H, Guo XL, Wan PB, Yu GH (2019) Conductive MXene nanocomposite organohydrogel for flexible, healable, low-temperature tolerant strain sensors. Adv Funct Mater 1904507. https://doi.org/10.1002/adfm.201904507
31. Lin F, Wang Z, Shen Y, Tang L, Zhang P, Wang Y, Chen Y, Huang B, Lu B (2019) Natural skin-inspired versatile cellulose biomimetic hydrogels. J Mater Chem A 7:26442-26455. https://doi.org/10.1039/C9TA10502F
32. Lin Q, Li H, Ji N, Dai L, Xiong L, Sun Q (2021) Self-healing, stretchable, and freezing-resistant hydroxypropyl starch-based double-network hydrogels. Carbohydr Polym 251:116982. https://doi.org/10.1016/j.carbpol.2020.116982
33. Ling Z, Edwards JV, Guo Z, Prevost NT, Nam S, Wu Q, French AD, Xu F (2018) Structural variations of cotton cellulose nanocrystals from deep eutectic solvent treatment: micro and nano scale. Cellulose 26:861-876. https://doi.org/10.1007/s10570-018-2092-9
34. Liu B, Yang D, Man H, Liu Y, Chen H, Xu H, Wang W, Bai L (2017) A green Pickering emulsion stabilized by cellulose nanocrystals via RAFT polymerization. Cellulose 25:77-85. https://doi.org/10.1007/s10570-017-1559-4
35. Liu S, Rao Z, Wu R, Sun Z, Yuan Z, Bai L, Wang W, Yang H, Chen H (2019) Fabrication of microcapsules by the combination of biomass porous carbon and polydopamine for dual self-healing hydrogels. J Agric Food Chem 67:1061-1071. https://doi.org/10.1021/acs.jafc.8b06241
36. Low LE, Siva SP, Ho YK, Chan ES, Tey BT (2020) Recent advances of characterization techniques for the formation, physical properties and stability of Pickering emulsion. Advances in Colloid and Interface Science 277:102117. https://doi.org/10.1016/j.cis.2020.102117
37. Lu C, Chen X (2020) All-temperature flexible supercapacitors enabled by antifreezing and thermally stable hydrogel electrolyte. Nano Lett 20:1907-1914. https://doi.org/10.1021/acs.nanolett.9b05148
38. Ma A, Wang G, Yang Z, Bai L, Chen H, Wang W, Yang H, Wei D, Yang L (2020) Fabrication of Janus graphene oxide hybrid nanosheets by Pickering emulsion template for self-healing nanocomposite hydrogels. Chem Eng J 385:123962. https://doi.org/10.1016/j.cej.2019.123962
39. Maestro A, Gutierrez JM, Santamaria E, Gonzalez C (2020) Rheology of water-in-water emulsions: Caseinate-pectin and caseinate-alginate systems. Carbohydr Polym 249:116799. https://doi.org/10.1016/j.carbpol.2020.116799
40. Navarchian AH, Najafipoor N, Ahangaran F (2019) Surface-modified poly(methyl methacrylate) microcapsules containing linseed oil for application in self-healing epoxy-based coatings. Prog Org Coat 132:288-297. https://doi.org/10.1016/j.porgcoat.2019.03.029

41. Oliveira FBd, Bras J, Pimenta MTB, Curvelo AAdS, Belgacem MN (2016) Production of cellulose nanocrystals from sugarcane bagasse fibers and pith. Ind Crop Prod 93:48-57. https://doi.org/10.1016/j.indcrop.2016.04.064
42. Phadke A, Zhang C, Arman B, Hsu CC, Mashelkar RA, Lele AK, Tauber MJ, Arya G, Varghese S (2012) Rapid self-healing hydrogels. P Natl Acad Sci USA 109:4383-4388. https://doi.org/10.1073/pnas.1201122109
43. Rao YL, Chortos A, Pfattner R, Lissel F, Chiu YC, Feig V, Xu J, Kurosawa T, Gu X, Wang C, He M, Chung JW, Bao Z (2016) Stretchable self-healing polymeric dielectrics cross-linked through metal-ligand coordination. J Am Chem Soc 138:6020-6027. https://doi.org/10.1021/jacs.6b02428
44. Shi W, Huang J, Fang R, Liu M (2020) Imparting functionality to the hydrogel by magnetic-field-induced nano-assembly and macro-response. ACS Appl Mater Interfaces 12:5177-5194. https://doi.org/10.1021/acsami.9b16770
45. Sirviö JA, Visanko M, Liimatainen H (2015) Deep eutectic solvent system based on choline chloride-urea as a pre-treatment for nanofibrillation of wood cellulose. Green Chem 17:3401-3406. https://doi.org/10.1039/c5gc00398a
46. Son D, Kang J, Vardoulis O, Kim Y, Matsuhisa N, Oh JY, To JW, Mun J, Katsumata T, Liu Y, McGuire AF, Krason M, Molina-Lopez F, Ham J, Kraft U, Lee Y, Yun Y, Tok JB, Bao Z (2018) An integrated self-healable electronic skin system fabricated via dynamic reconstruction of a nanostructured conducting network. Nat Nanotechnol 13:1057-1065. https://doi.org/10.1038/s41565-018-0244-6
47. Song F, Gong J, Tao Y, Cheng Y, Lu J, Wang H (2021) A robust regenerated cellulose-based dual stimuli-responsive hydrogel as an intelligent switch for controlled drug delivery. Int J Biol Macromol 176:448-458. https://doi.org/10.1016/j.ijbiomac.2021.02.104
48. Suryanarayana C, Rao KC, Kumar D (2008) Preparation and characterization of microcapsules containing linseed oil and its use in self-healing coatings. Prog Org Coat 63:72-78. https://doi.org/10.1016/j.porgcoat.2008.04.008
49. Taylor DL, In Het Panhuis M (2016) Self-healing hydrogels. Adv Mater 28:9060-9093. https://doi.org/10.1002/adma.201601613
50. Wang G, Xi M, Bai L, Liang Y, Yang L, Wang W, Chen H, Yang H (2019a) Pickering emulsion of metal-free photoinduced electron transfer-ATRP stabilized by cellulose nanocrystals. Cellulose 26:5947-5957. https://doi.org/10.1007/s10570-019-02528-4
51. Wang J, Zhang D, Chu F (2020) Wood-derived functional polymeric materials. Adv Mater 2001135. https://doi.org/10.1002/adma.202001135
52. Wang Q, Pan X, Lin C, Lin D, Ni Y, Chen L, Huang L, Cao S, Ma X (2019b) Biocompatible, self-wrinkled, antifreezing and stretchable hydrogel-based wearable sensor with PEDOT: sulfonated lignin as conductive materials. Chem Eng J 370:1039-1047. https://doi.org/10.1016/j.cej.2019.03.287
53. Wei P, Chen T, Chen G, Liu H, Mugaanire IT, Hou K, Zhu M (2020) Conductive self-healing nanocomposite hydrogel skin sensors with antifreezing and thermoresponsive properties. ACS Appl Mater Interfaces 12:3068-3079. https://doi.org/10.1021/acsami.9b20254

54. Wei Z, He J, Liang T, Oh H, Athas J, Tong Z, Wang C, Nie Z (2013) Autonomous self-healing of poly(acrylic acid) hydrogels induced by the migration of ferric ions. Polym Chem 4:4601-4605. https://doi.org/10.1039/c3py00692a
55. Wu J, Ma GH (2016) Recent studies of Pickering emulsions: particles make the difference. Small 12:4633-4648. https://doi.org/10.1002/smll.201600877
56. Xu Y, Rong Q, Zhao T, Liu M (2020) Anti-freezing multiphase gel materials: Bioinspired design strategies and applications. Giant 2:100014. https://doi.org/10.1016/j.giant.2020.100014
57. Yang Y, Guan L, Li X, Gao Z, Ren X, Gao G (2019) Conductive organohydrogels with ultrastretchability, antifreezing, self-Healing, and adhesive properties for motion detection and signal transmission. ACS Appl Mater Interfaces 11:3428-3437. https://doi.org/10.1021/acsami.8b17440
58. Yu Q, Qin Z, Ji F, Chen S, Luo S, Yao M, Wu X, Liu W, Sun X, Zhang H, Zhao Y, Yao F, Li J (2021) Low-temperature tolerant strain sensors based on triple crosslinked organohydrogels with ultrastretchability. Chem Eng J 404:126559. https://doi.org/10.1016/j.cej.2020.126559
59. Zhang B, Zhang Z, Kapar S, Ataeian P, Da Silva Bernardes J, Berry R, Zhao W, Zhou G, Tam KC (2019) Microencapsulation of phase change materials with polystyrene/cellulose nanocrystal hybrid shell via Pickering emulsion polymerization. ACS Sustain Chem Eng 7:17756-17767. https://doi.org/10.1021/acssuschemeng.9b04134
60. Zhang X, Wang Y, Luo X, Lu A, Li Y, Li B, Liu S (2018) O/W Pickering emulsion templated organo-hydrogels with enhanced mechanical strength and energy storage capacity. ACS Applied Bio Materials 2:480-487. https://doi.org/10.1021/acsabm.8b00674
61. Zhao H, Liu M, Zhang Y, Yin J, Pei R (2020) Nanocomposite hydrogels for tissue engineering applications. Nanoscale 12:14976-14995. https://doi.org/10.1039/d0nr03785k

Figures

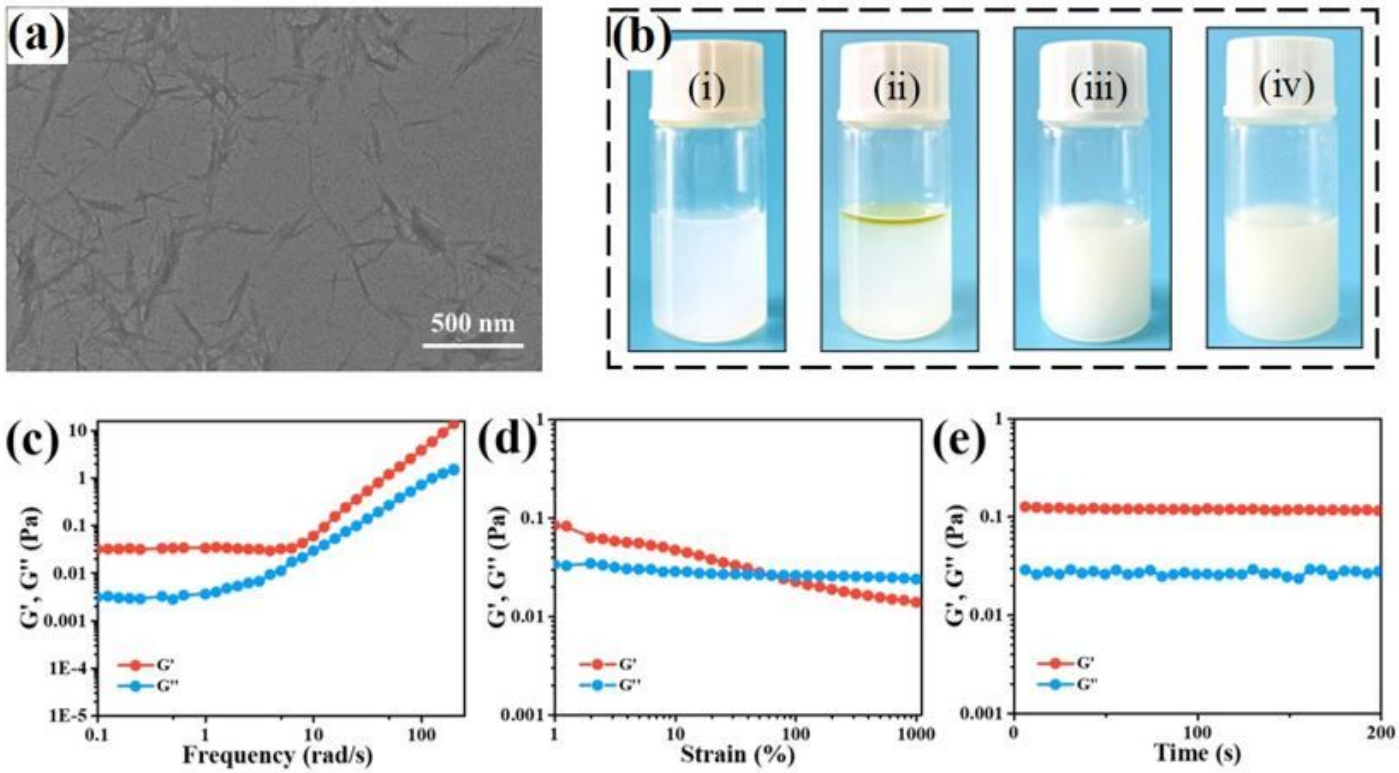

Figure 1

(a) TEM image of CNCs. (b) The preparation process of Pickering emulsions was reflected in optical images. (□) CNCs suspension; (□) Adding LO; (□) Pickering emulsions; (□) After leaving for 1 day at room temperature. (c) Rheology test of Pickering emulsions under frequency sweep data from 0.1 to 200 rad/s at 1%, 25 °C. (d) Strains sweep data from 1 to 1000% at 10 rad/s, 25 °C. (e) Time sweep data for 200 s at 1%, 10 rad/s and 25 °C (G'= storage modulus, G"=loss modulus)

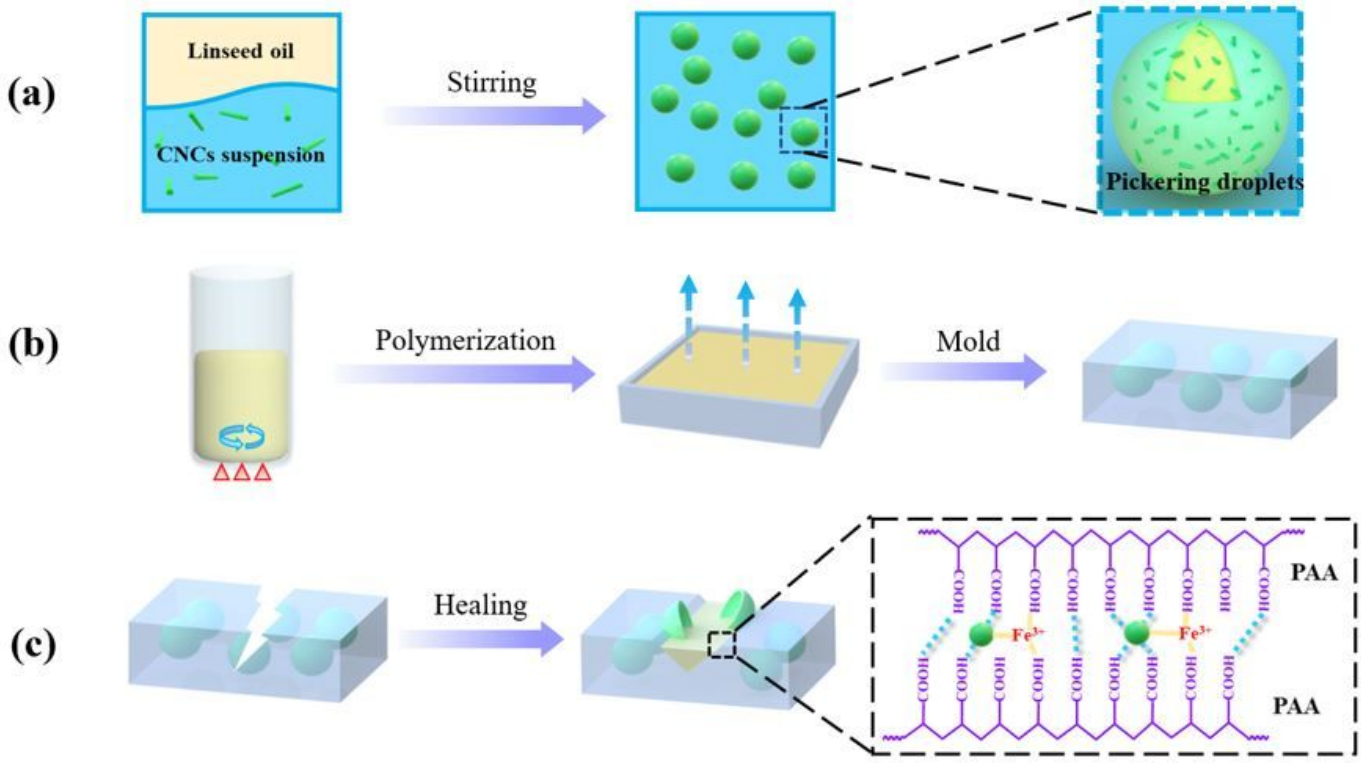

Figure 2

Preparation process of (a) CNCs-stabilized Pickering emulsions and (b) nanocomposite hydrogels. (c) Mechanism of dual self-healing interactions

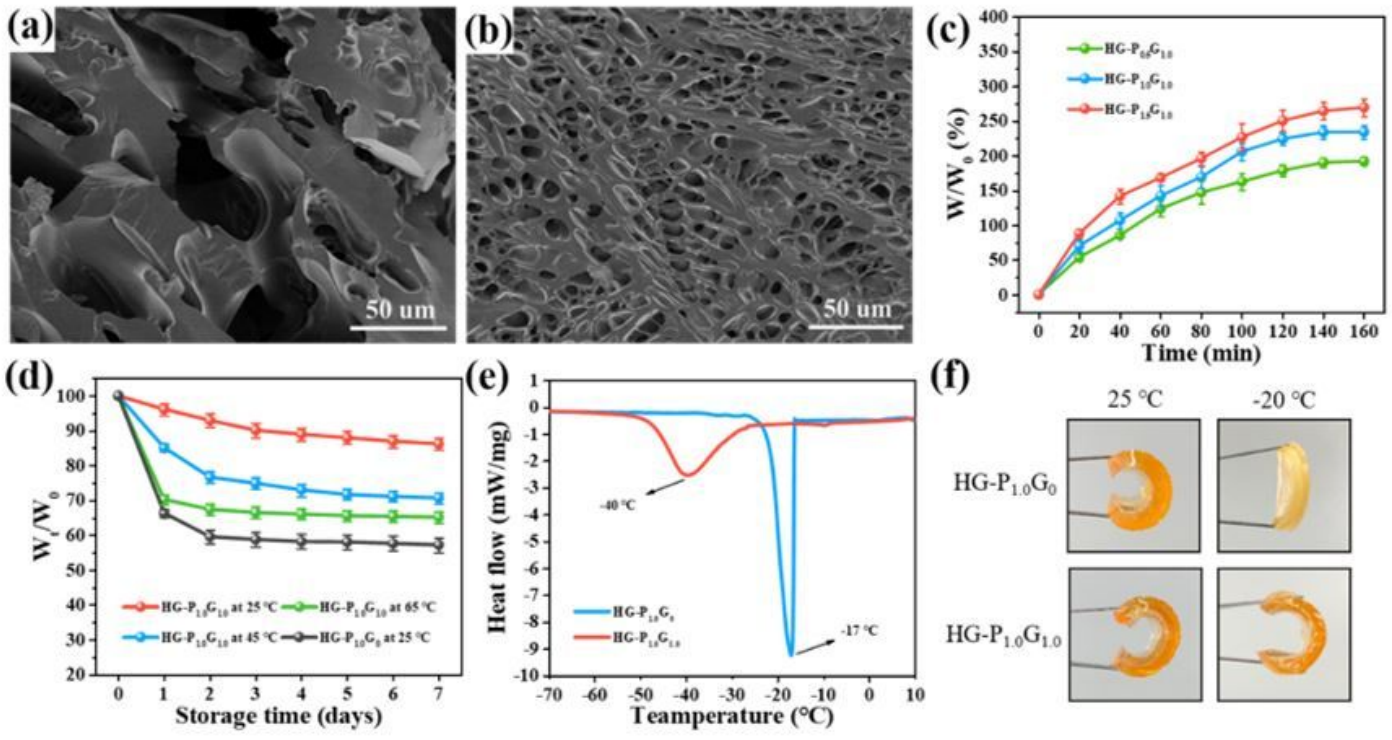

Figure 3

SEM images of cross-sectional morphology of (a) HG-P0G0, (b) HG-P1.0G1.0. (c) Swelling kinetics curves of HG-P0.5G1.0, HG-P1.0G1.0 and HG-P1.5G1.0 immersed in distilled water at room temperature. (d) Water retention kinetics curves of HG-P1.0G0 at 25 ℃ and HG-P1.0G1.0 at 25, 45 and 65 ℃ for 7 days. (e) DSC thermograms of HG-P1.0G0 and HG-P1.0G1.0 from 10 to -70 ℃ at a cooling rate of 10 ℃/min. (f) Photographs of HG-P1.0G0 and HG-P1.0G1.0 showing their flexibility at 25 ℃ and -20 ℃

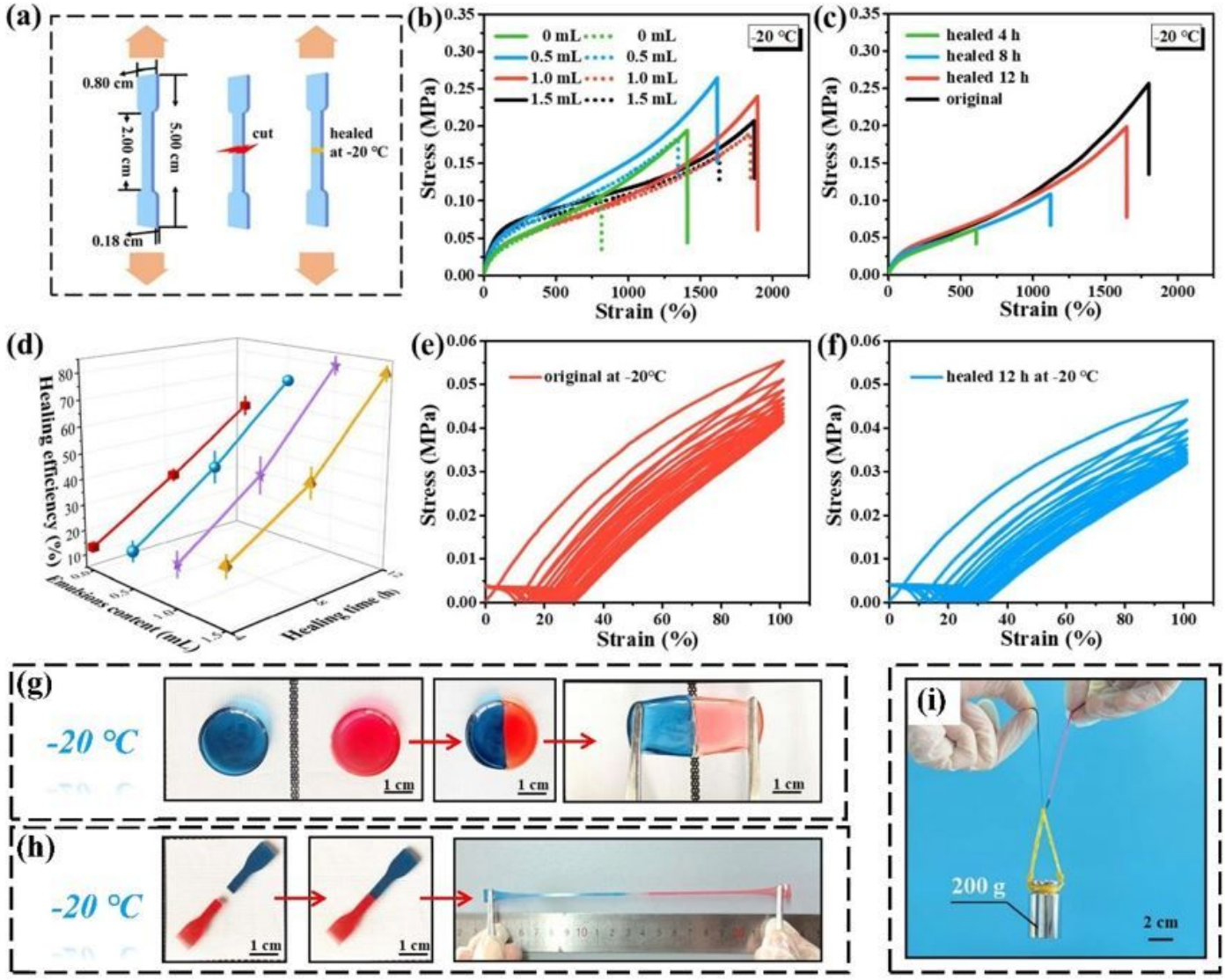

Figure 4

(a) Diagrammatic drawing of the standard samples for tensile testing. (b) Tensile stress-strain curves with 0, 0.5, 1.0 and 1.5 mL of Pickering emulsions before (solid line) and after self-healing (dotted line) at -20 ℃ for 12 h. (c) Tensile stress-strain curves of HG-P1.0G1.0 for 0, 4, 8 and 12 h at -20 ℃. (d) Healing efficiency with different contents of Pickering emulsions and different time. (e) The original and (f) self-healing loading-unloading stress-strain curves of HG-P1.0G1.0 under 100% strain for ten successive cycles. (g) The dyed hydrogels were prepared in circle shapes (Φ=2.5 cm) and healed for stretch test. (h)

The dyed hydrogels were prepared in dumbbell shapes (L=5.0 cm) and healed for stretch test. (i) Heavy loading test with a weight of 200 g

Supplementary Files

This is a list of supplementary files associated with this preprint. Click to download.

- Supportinginformation.docx